



Uncoupling the size and support effects of Ni catalysts for dry reforming of methane

Joung Woo Han^{a,1,2}, Jun Seong Park^{a,1,3}, Min Suk Choi^b, Hyunjoo Lee^{b,*}

^a Department of Chemical and Biomolecular Engineering, Yonsei University, Seoul 120-749, Republic of Korea

^b Department of Chemical and Biomolecular Engineering, Korea Advanced Institute of Science and Engineering, Daejeon 305-701, Republic of Korea



ARTICLE INFO

Article history:

Received 12 July 2016

Received in revised form

21 September 2016

Accepted 24 October 2016

Available online 24 October 2016

Keywords:

Dry reforming of methane

Ni catalysts

Nanoparticles

Stability

Metal oxide

ABSTRACT

The dry reforming of methane (DRM: $\text{CH}_4 + \text{CO}_2 \leftrightarrow 2\text{H}_2 + 2\text{CO}$) can be a good way to utilize greenhouse gases for the production of valuable syn-gas. Ni-based catalysts have been used for this reaction; however, the Ni size effect and support effect were highly coupled and therefore could not be observed separately. Here, a unique catalyst in which the Ni nanoparticle size and support can be varied independently was devised. Highly uniform Ni nanoparticles with sizes of 2.6, 5.2, 9.0, and 17.3 nm were tested for DRM at 800 °C without a significant change in the Ni size, and overlayers of various metal oxides, including SiO_2 , Al_2O_3 , MgO , ZrO_2 , TiO_2 , were tested with the 5.2 nm of Ni nanoparticles. The dependence of the CH_4 or CO_2 turnover frequency on the Ni size and support was evaluated separately. The 2.6 nm Ni nanoparticles showed 4.1 times higher methane turnover frequency than those with a size of 17.3 nm. When various metal oxide overlayers were tested with the same 5.2 nm Ni, Al_2O_3 exhibited 4.3 times higher methane turnover frequency than SiO_2 . The independent observation of the effects of the Ni nanoparticle size and support will provide valuable guidelines for designing effective methane dry reforming catalysts.

© 2016 Elsevier B.V. All rights reserved.

1. Introduction

Methane conversion has received much attention as shale gas has been developed. The dry reforming of methane is an especially interesting reaction that converts two of the most important greenhouse gases—methane and carbon dioxide—into syn-gas, which is a mixture of hydrogen and carbon monoxide. Syn-gas is a basic material that can be used to synthesize various chemicals and fuels [1–4]. Ni catalysts are the most widely used for reforming reactions. Compared to precious-metal catalysts such as Pt, Ru, and Rh, Ni is much cheaper and exhibits high activity toward methane conversion. However, unlike precious-metal catalysts, Ni typically suffers from severe coke formation [5,6]. Whereas coke formation can be minimized in steam reforming ($\text{CH}_4 + \text{H}_2\text{O} \leftrightarrow 3\text{H}_2 + \text{CO}$) through the use of excessive amounts of steam, the coke formation becomes more serious in dry reforming because CO_2 also contributes to coke deposition.

Various methods have been used to minimize coke deposition on Ni catalysts. One of the most popular methods is to minimize the Ni particle size. Carbon deposition on a Ni surface is known to necessitate Ni ensembles, and large Ni particles cause more severe coke deposition [7–9]. However, because the dry reforming reaction typically occurs at very high temperatures, the initially small Ni particles become sintered and the size of the Ni domains eventually becomes large with heavy coke deposition. Strong metal-support interactions are often used to maintain the small size of the Ni particles at high reaction temperatures. When strong interactions occur between the Ni particles and their support (e.g., Al_2O_3 , MgO , or CeO_2), the interaction might cause the size of the Ni particles to decrease during the synthesis and also contribute to minimizing the aggregation because the support tends to retain Ni particles even at high temperatures [10–18]. However, this effect for size preservation is limited, and most Ni particles inevitably become larger after long reactions. This enlargement blurs the effect of Ni particle size on the activity for dry reforming. Smaller Ni particles are usually considered more advantageous because of their higher surface area and better coke resistance; however, Baudouin et al. claimed that the turnover frequency, which is the activity per available surface Ni atom per unit time, is independent of Ni particle size for the dry reforming of methane at 500 °C [19]. They argued, however, that the Ni particle size increased significantly after the reaction despite the use of a relatively low reaction temperature

* Corresponding author.

E-mail address: azhyun@kaist.ac.kr (H. Lee).

¹ J. W. Han and J. S. Park contributed equally to this work.

² The current address: Hanwha Chemical R&D Center, Daejeon, Republic of Korea.

³ The current address: Lotte Chemical Corporation, Daejeon, Republic of Korea.

and this increase in size precluded proper evaluation of the effect of particle size.

The supports are also known to significantly affect the catalytic property of metals by altering their electronic structure [20–23]. CO₂ is more readily adsorbed onto basic supports such as MgO [23–27]. When oxygen ions can transport through metal oxide supports such CeO₂ or ZrO₂, they can also help burn out the deposited coke [20,28–33]. These support effects are, in fact, highly coupled with the size effect [22,34,35]. Numerous authors who have reported the potential support effect have also attributed the enhancement in activity and coke resistance to the size effect. Raberg et al. reported the influence of supports for propane dry reforming over Ni-based catalysts [35]; however, their catalysts contained Ni particles with different sizes, e.g., 4 nm in the case of Ni/MgAlO_x and 10 nm in the case of Ni/CaO. This difference in size for various supports is almost inevitable when the supported catalysts are prepared via the synthetic method of wet impregnation and subsequent calcination. The low activity of Ni/CaO can therefore be due either to the large Ni size or to the support effect of the CaO, and the relative importance of these two aspects is unclear. Independently observing the size and support effect in dry reforming can provide researchers with valuable insight to design better catalysts.

We previously showed that small-sized Ni nanoparticles (~5 nm) catalyzed the dry reforming of methane without sintering and coke formation when the Ni nanoparticles were protected by a silica overlayer [36]. Because the size of the Ni nanoparticles did not substantially change, this catalyst can be used to evaluate the exact effect of Ni particle size on the dry reforming of methane. Here, we prepared 2.6, 5.2, 9.0, and 17.3 nm Ni nanoparticles and estimated the size effect on the turnover frequency while minimizing the sintering of those nanoparticles during the DRM reaction at 800 °C. Additionally, different metal oxides (SiO₂, Al₂O₃, MgO, ZrO₂, and TiO₂) were used to coat Ni nanoparticles of a single size (5.2 nm), and the effect of the interaction between the various metal oxide overlayers and the Ni particles on the dry reforming was evaluated.

2. Experimental section

Scheme 1 illustrates the catalysts that allow the effects of the size and support to be evaluated independently. The synthetic methods are detailed below.

2.1. Synthesis of Ni nanoparticles

Various sizes of Ni nanoparticles were prepared following previously reported methods [37,38]. Nickel acetylacetonate (Ni(acac)₂; 95%, Aldrich), trioctylphosphine (TOP; 90%, Aldrich), and oleylamine (70%, Aldrich) were added into a three-necked flask, and the flask was heated in N₂ and aged at the same temperature. The amounts of each chemical and the specific synthesis conditions are shown in Table S1 for each Ni particle size. The resulting nanoparticles were washed twice with ethanol and then redispersed in 15 mL ethanol.

2.2. Immobilizing Ni nanoparticles on the silica spheres (Ni/SiO₂)

Silica spheres with a size of ~400 nm were prepared following previously reported methods [39,40]. First, 45 mL ethanol (99.9% Samchun), 5 mL deionized (DI) water, 5 mL ammonium hydroxide (28%, Duksan), and 5 mL tetraethylorthosilicate (TEOS, 98%, Aldrich) were added into a flask and stirred for 6 h, and the solution was then washed twice with ethanol. The washed silica spheres were redispersed in 15 mL ethanol. The dispersion of silica spheres in ethanol (5 mL) and 0.15 mL 3-mercaptopropyltrimethoxysilane (MPTMS, 95%, Aldrich) were added into a vial and ultrasonicated

for 10 min. Then, the resultant was aged for 2 h at 80 °C. The functionalized silica was washed with ethanol twice and re-dispersed in 13 mL ethanol. The functionalized SiO₂ solution and appropriate amounts of the Ni nanoparticle solution were added into a vial and ultrasonicated for 1 h. Then, the solid was collected by centrifugation after washing with ethanol. After drying at 80 °C for 12 h, the Ni/SiO₂ powder was obtained. The Ni weight percentage ranged from 0.15 wt% to 0.35 wt% to locate Ni nanoparticles separately with the appropriate distance.

2.3. SiO₂ coating on the Ni/SiO₂ (Ni/SiO₂@SiO₂)

Ni/SiO₂ powders (350 mg) were sonicated in 9 mL ethanol. Then, 8 mL ethanol, 0.6 mL ammonium hydroxide (28%, Duksan), 300 mg cetyltrimethylammonium bromide (CTAB, 95%, Aldrich), and the powder solution were added into a vial. Under vigorous stirring, 1.5 mL TEOS was injected dropwise into the vial. The solution was stirred for an additional 5 h. The solids were washed twice with ethanol, and the Ni/SiO₂@SiO₂ catalysts were collected by centrifugation. The precipitates were dried at 80 °C for 12 h and then calcined at 550 °C for 2 h in air to remove the CTAB.

2.4. Coating other metal oxides on Ni/SiO₂ (Ni/SiO₂@M_xO_y, M=Al, Ti, Mg, or Zr)

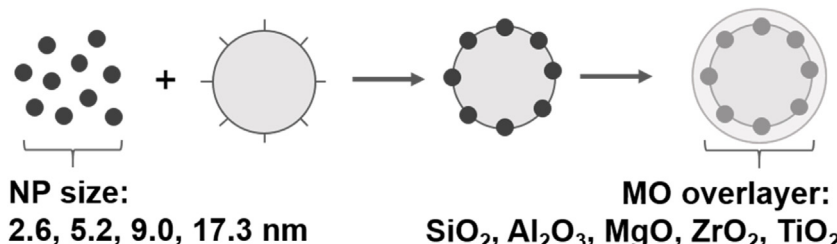
Ni/SiO₂ (Ni size: 5.2 nm) powders (350 mg) were sonicated in 9 mL ethanol. The Ni/SiO₂ dispersion, CTAB, water, and metal oxide precursor were mixed with vigorous stirring. The metal oxide precursors, their amounts, and the specific synthesis conditions are shown in Table S2 for each metal oxide coating. After synthesis, the coated Ni/SiO₂ catalysts were collected by centrifugation after washing with ethanol. The precipitates were dried at 80 °C for 12 h, and then calcined at 550 °C for 2 h in air to remove the CTAB. The precipitates were also thermally treated in hydrogen at 800 °C for 1 h and in nitrogen at 800 °C for an additional 4 h to reduce the Ni species and to stabilize the coated overlayers.

2.5. Dry reforming of methane (DRM)

The DRM was performed in a quartz glass fixed-bed reactor at atmospheric pressure and 800 °C. A total of 100 mg of the catalyst was located inside the reactor. The reactant gas was introduced with a flow rate of 9 mL/min of CH₄, 9 mL/min of CO₂, and 2 mL/min of N₂. The nitrogen was used as an internal standard. The outlet gas was analyzed with an online gas chromatograph (GC, Younglin GC 6000) equipped with a thermal conductivity detector and molecular sieve 5A and Porapak N as the column.

2.6. Characterizations

Transmission electron microscopy (TEM; Jeol JEM-2100 or Philips Technai-20), high angle annular dark field scanning TEM (HAADF-STEM; Jeol JEM-ARM200F) and field emission STEM (FE-STEM; HITACHI HD-2300) images were obtained at 200 kV to observe visual changes. The amount of actual Ni active sites was estimated from CO-TPD (temperature-programmed desorption) using equipment custom made in the lab with a methanizer and a flame ionization detector (FID). Each catalyst was introduced into a U-shaped quartz cell and reduced at 800 °C for 2 h. The catalyst was cooled to room temperature under Ar flow, then 99.99% CO flowed through the sample at a rate of 20 mL/min for 2 h. Ar flowed through the sample to remove any physisorbed CO until the CO peak was not observed. The desorbed CO was measured by the FID while the temperature increased. Temperature-programmed reduction (TPR), temperature-programmed oxidation (TPO), and CO₂-TPD were performed on a BELCAT-B (BEL, Japan) equipped



Scheme 1. Synthetic strategy for catalysts where size effect and support effect can be observed separately.

with a thermal conductivity detector. Each catalyst was loaded and pre-treated under Ar flow at 250 °C for 2 h, cooled down to room temperature, then the 5% H₂/Ar or 20% O₂/He gas was introduced and heated to 1000 °C at a ramping rate of 10 °C/min for TPR or TPO. For CO₂-TPD, each catalyst was loaded and reduced at 800 °C for 2 h, and cooled down to room temperature under He flow, then exposed to 99.999% CO₂ for 1 h. After purging physically adsorbed CO₂ with He flow, temperature increased at a rate of 10 °C/min. The amounts of Ni in the catalysts were measured by inductively coupled plasma optical emission spectroscopy (ICP-OES; ICP-OES 720, Agilent) after dissolving the catalyst completely in aqua regia solution.

3. Results and discussion

3.1. Ni size effect on the DRM

The Ni nanoparticles were synthesized using the colloidal method with diameters of 2.6 ± 0.4, 5.2 ± 0.4, 9.0 ± 0.4, and 17.3 ± 2.3 nm, as shown in Fig. 1. Their size distributions showed little overlap, enabling the observation of each size's effect on the reaction. Then, the catalysts with the structure shown in Scheme 1 were prepared for the various sizes of Ni nanoparticles and the SiO₂ overlayer. Fig. 2 shows the TEM images of the catalyst after each step and HAADF-STEM images after the reaction (i.e., TEM images after Ni deposition onto the silica spheres ((a)–(d)), after the formation of the SiO₂ overlayer and subsequent calcination ((e)–(h)), and after the DRM reaction at 800 °C for 100 h ((i)–(l)); and HAADF-STEM images collected after the DRM reaction ((m)–(p))). Fig. 2(a)–(d) shows that the Ni nanoparticles were immobilized on the thiol-functionalized silica spheres. The nanoparticles were not finely distributed on the silica surface but rather existed as Ni aggregates without the functionalization. The Ni nanoparticles showed no aggregation after calcination, as shown in Fig. 2(e)–(h). No large Ni particles were observed. More encouragingly, the Ni nanoparticles also showed no aggregation after the reaction at 800 °C for 100 h, as shown in Fig. 2(i)–(l). The STEM images in Figs. 2(m)–(p) were used to estimate the nanoparticle size after the reaction. The Ni nanoparticles after the reaction exhibited only small increases in size: from 2.6 to 3.6 nm, 5.2 to 5.5 nm, 9.0 to 9.4 nm, and 17.3 to 18.7 nm. The various sizes of the Ni nanoparticles still showed only a slight overlap after the reaction, as shown in Fig. S1. It should be noted that the porous silica overlayer collapsed into the non-porous layer after the DRM reaction, exhibiting much smaller Brunauer–Emmett–Teller (BET) surface areas of 4.0, 4.2, 6.7, and 6.2 m²/g from 30.7, 37.6, 33.9, and 34.0 m²/g for the 2.6, 5.2, 9.0, and 17.3 nm Ni nanoparticles, respectively.

The TPR results in Fig. 3 show that all sizes of the Ni nanoparticles were completely reduced below 500 °C, although smaller Ni nanoparticles were reduced at higher temperatures. The activation energy for methane conversion was estimated as 93.5 kJ/mol from the Arrhenius plot shown in Fig. S2, which is quite close to the value reported previously [41]. The CH₄ and CO₂ conversions at 800 °C are shown in Fig. 4. The CO₂ conversion was greater than the

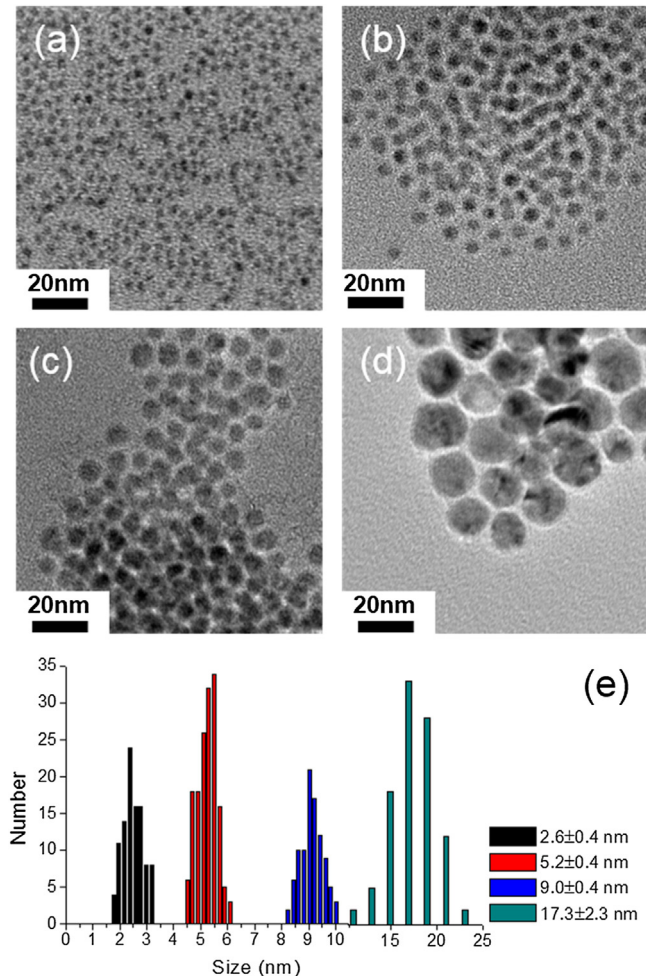


Fig. 1. TEM images of a) 2.6 nm, b) 5.2 nm, c) 9.0 nm and d) 17.3 nm Ni nanoparticles. The size distribution of each sized particle is shown in e).

CH₄ conversion, indicating that the reverse water-gas shift reaction ($\text{H}_2 + \text{CO} \rightarrow \text{CO} + \text{H}_2\text{O}$) occurred to a significant extent, resulting in H₂/CO ratios less than one. Because the overlayers covered some part of the Ni surface, the conversions do not necessarily reflect the intrinsic activity; we therefore evaluated the turnover frequency, which is the activity per Ni surface atom per unit time. The number of Ni surface atoms available for the DRM was measured using CO-TPD. Table 1 shows the number of surface Ni sites and the turnover frequencies for the DRM before and after the reaction. The number of CO uptakes, which is the number of surface Ni sites, increased slightly after 100 h of reaction at 800 °C because the silica overlayer became more open after the high-temperature reaction. Fig. 5 clearly shows that the turnover frequency for the methane conversion on the Ni surface was dependent on the size of the Ni nanoparticles. The smallest nanoparticles (2.6 nm) exhib-

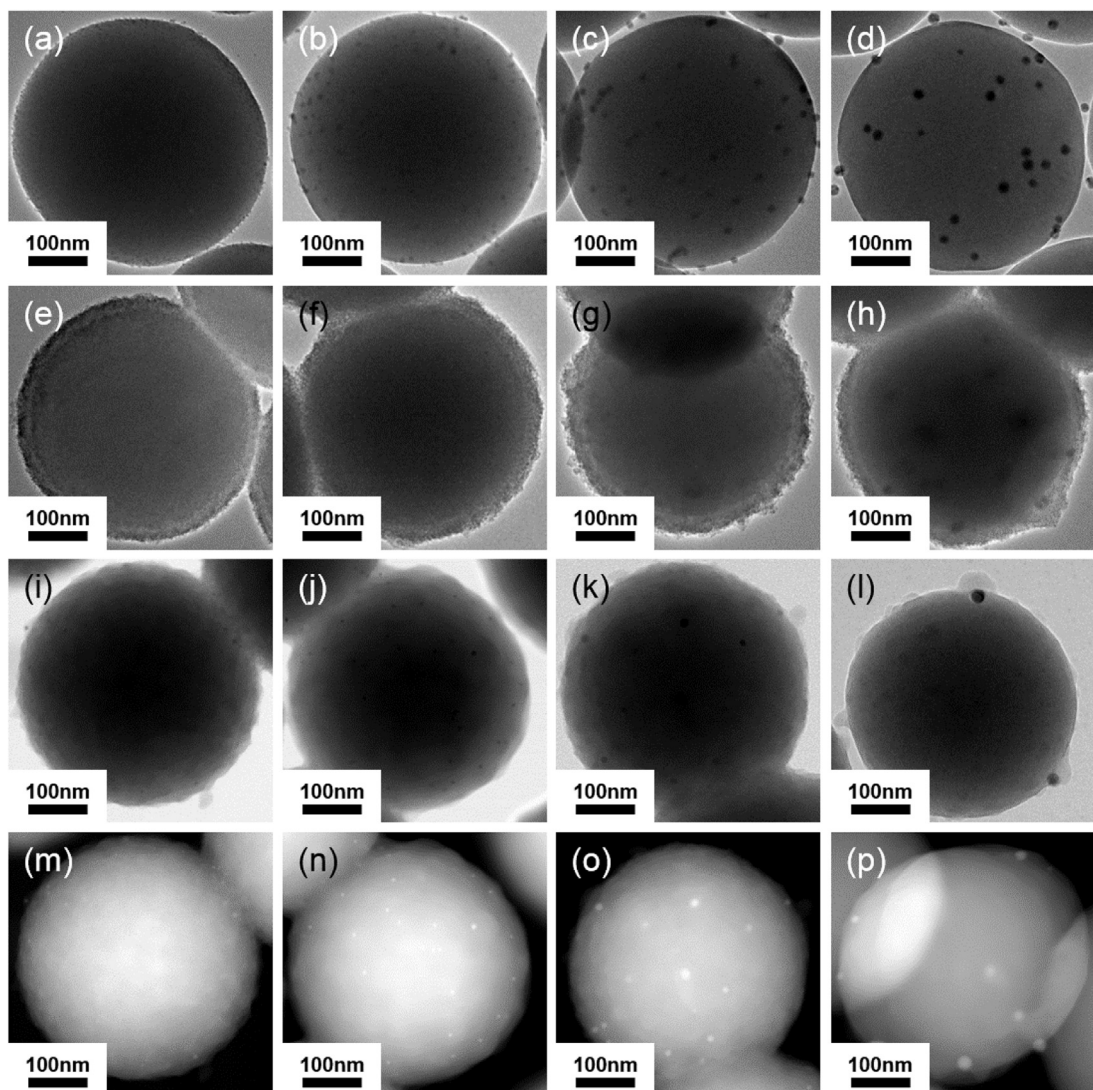


Fig. 2. TEM images of a–d) each Ni nanoparticle deposited on silica, e–h) SiO_2 -overlayer-coated Ni catalysts, i–l) SiO_2 -overlayer-coated Ni catalysts after the DRM at 800°C for 100 h m–p) HAADF-STEM images of the catalysts after the DRM. The 1 st through 4 th columns from left to right show the 2.6 nm, 5.2 nm, 9.0 nm and 17.3 nm Ni nanoparticles, respectively.

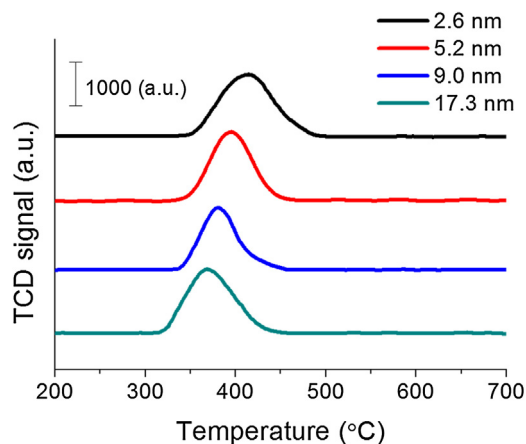


Fig. 3. TPR results of the catalysts with various Ni nanoparticle sizes.

ited a CH_4 turnover frequency 4.1 times greater than that of the largest nanoparticles (17.3 nm). The decrease in turnover frequency was attenuated as the size of the Ni nanoparticles increased. The

Table 1
The effect of Ni nanoparticle size on CH_4 and CO_2 conversions for $\text{Ni}/\text{SiO}_2@\text{SiO}_2$ catalysts.^a

	2.6 nm	5.2 nm	9.0 nm	17.3 nm
Ni content (wt%)	0.21	0.32	0.16	0.16
Initial CO uptakes ($\mu\text{mol/g}$)	0.42	0.81	0.59	0.46
Initial CH_4 conversion (%)	39.0	38.3	18.8	10.4
Initial CO_2 conversion (%)	66.0	62.2	37.8	24.0
Initial $\text{TOF}_{\text{CH}_4} (\text{s}^{-1})$	61.7	31.8	21.2	15.1
Initial $\text{TOF}_{\text{CO}_2} (\text{s}^{-1})$	104.4	51.6	42.5	34.8
Final CO uptakes ($\mu\text{mol/g}$)	0.54	0.93	0.67	0.54
Final CH_4 conversion (%)	36.7	36.8	18.8	12.6
Final CO_2 conversion (%)	62.4	61.6	35.4	26.6
Final $\text{TOF}_{\text{CH}_4} (\text{s}^{-1})$	44.4	26.5	18.8	15.6
Final $\text{TOF}_{\text{CO}_2} (\text{s}^{-1})$	77.3	44.4	35.4	32.9

^a Surface Ni sites and turnover frequencies were compared before and after the DRM reaction. The reactions were performed at 800°C for 100 h.

turnover frequency showed little change after the reaction for 100 h. The turnover frequency for the various Ni nanoparticle sizes was compared with the surface fraction of low coordinated atoms at vertexes and edges. The surface fraction of vertexes and edges was estimated to be 0.314 for 2.6 nm and 0.048 for 17.3 nm following

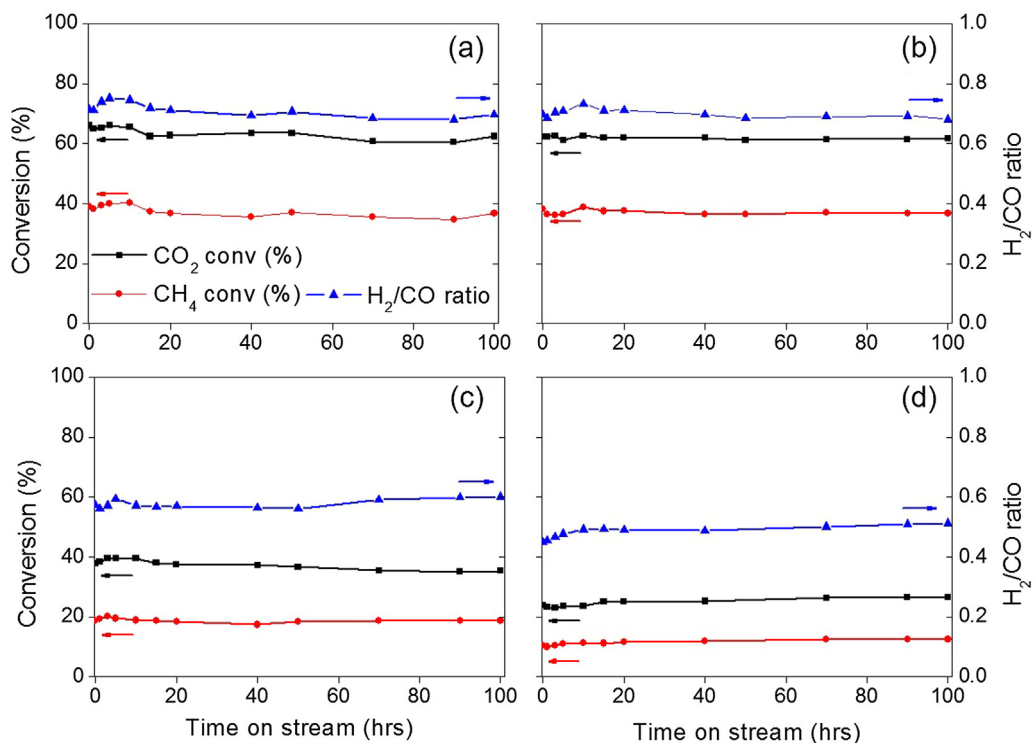


Fig. 4. CH₄ and CO₂ conversion and H₂/CO ratio results over a) 2.6 nm, b) 5.2 nm, c) 9.0 nm and d) 17.3 nm Ni catalysts as a function of time on stream (reaction conditions; 800 °C, 100 mg catalyst, the flow rates of CH₄, CO₂, and N₂ were 9, 9, and 2 mL/min, respectively.).

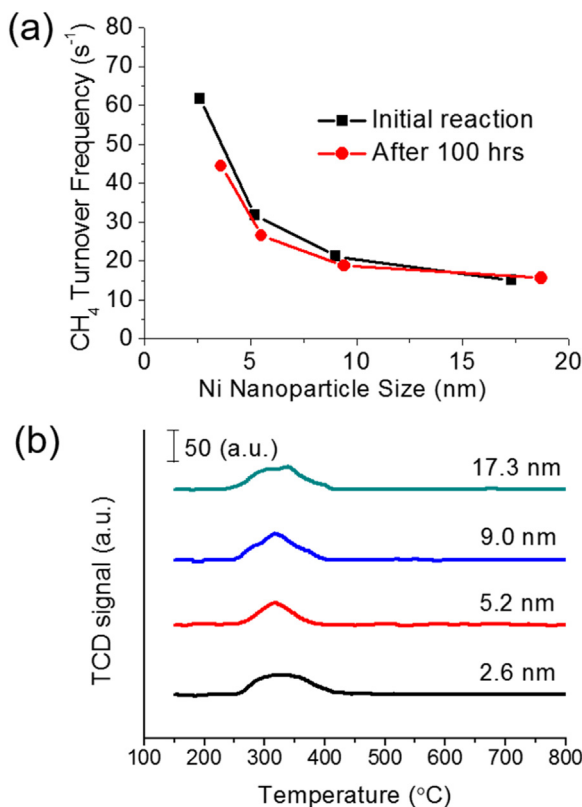


Fig. 5. (a) Dependence of CH₄ turnover frequency on the Ni nanoparticle size, (b) TPO results after running the DRM reaction at 800 °C for 100 h.

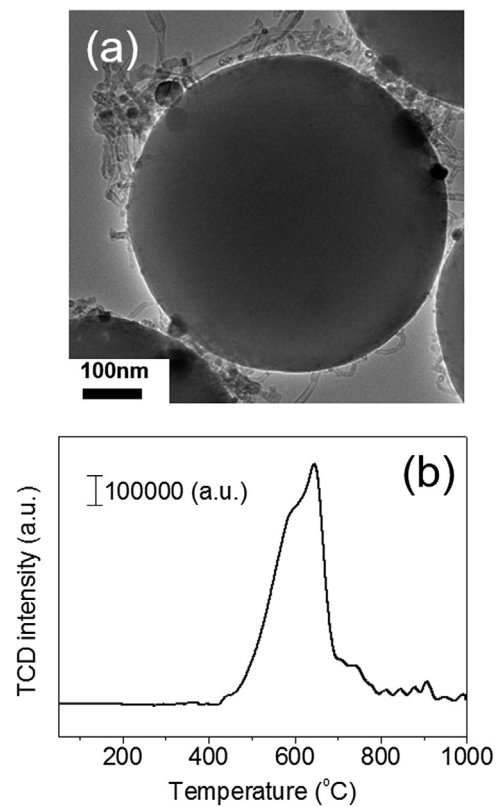


Fig. 6. (a) TEM image and (b) TPO results of the Ni/SiO₂ catalyst without an overlayer (Ni NP size: 5.2 nm) after the DRM reaction at 800 °C.

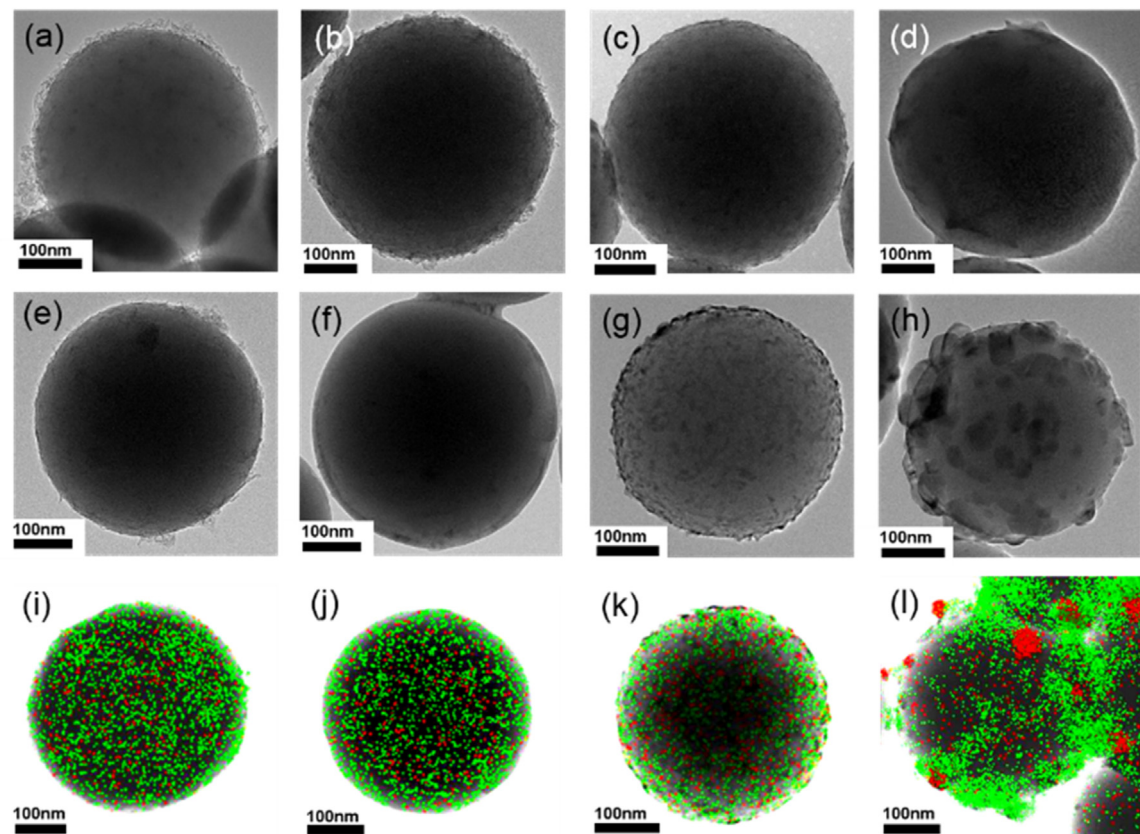


Fig. 7. TEM images of a–d) as-made metal oxide overlayers formed on Ni/SiO₂ samples, e–h) after reduction at 800 °C for 1 h under hydrogen flow and additional stabilization for 4 h under nitrogen flow, i–l) the overlapped elemental mapping by HAADF-STEM with metal (Al, Mg, Zr, or Ti; green) and Ni (red) for the catalysts after reduction and stabilization. The 1st through 4th columns from left to right show the Al₂O₃, MgO, ZrO₂, and TiO₂ overlayers, respectively. (For interpretation of the references to colour in this figure legend, the reader is referred to the web version of this article.)

the Van Hardeveld and Hartog method [42]. This surface fraction was therefore 6.5 times higher for the 2.6 nm nanoparticles. Fig. S3 shows that the change in turnover frequency corresponds well with the change in the surface fraction of edges and vertexes.

TPO was performed for the catalyst samples after the 100 h DRM reaction. Fig. 5(b) shows a peak at 250–400 °C only, which indicates oxidation of the Ni surface, and no peak at higher temperature. Filamentous carbon was not observed in the TEM images, no Raman D or G peaks were observed, and no typical TPO peaks to indicate coke oxidation above 400 °C were observed. These results confirm that no carbon was deposited when the size of Ni nanoparticles was increased up to 17.3 nm. However, the possibility cannot be excluded that the silica overlayer further suppressed the coke formation at the Ni surface. When Ni/SiO₂ sample was used as a catalyst without a silica overlayer, the Ni nanoparticles were severely aggregated, and large Ni particles with ~100 nm domain size were often observed. In addition, filamentous cokes were heavily formed with a large TPO peak at ~650 °C, as shown in Fig. 6.

3.2. Support effect on the DRM

Different types of metal oxide overlayers were formed via sol-gel methods on the Ni nanoparticles (5.2 nm) immobilized on silica spheres. Fig. 7 shows Al₂O₃, ZrO₂, MgO, and TiO₂ overlayers synthesized on Ni/SiO₂ catalysts. The as-made metal oxide overlayers were formed conformably, as shown in Fig. 7(a)–(d). The TPR results in Fig. 8 show that the Ni nanoparticles were reduced at higher temperatures than the SiO₂ overlayer, indicating that the interaction between the Ni and metal oxide overlayer was stronger. Not all of the metal oxides were stable at 800 °C, however. When the

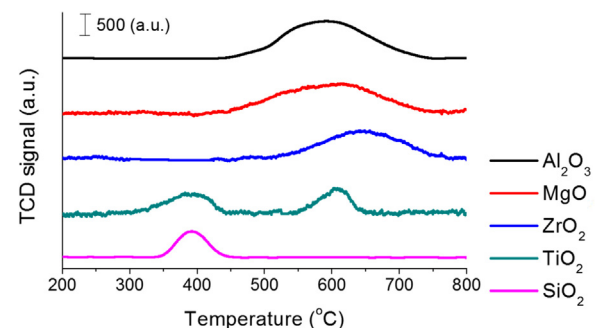


Fig. 8. TPR results for the metal oxide overlayer samples.

catalysts were reduced at 800 °C for 1 h under hydrogen flow and treated at the same temperature for an additional 4 h under nitrogen flow, the Al₂O₃, ZrO₂, and MgO overlayers exhibited only a slight change, as shown by the TEM images in Fig. 7(e)–(g); however, the TiO₂ overlayer showed significant crystallization, with distinct oxide domains, as shown in Fig. 7(h). The Ni nanoparticles could not be clearly observed for the metal oxide overlayers by HAADF-STEM imaging, unlike the Ni nanoparticles with the SiO₂ overlayer. Instead, the elemental distribution was observed by STEM, as shown in Figs. 7(i)–(l). The Al₂O₃, ZrO₂, and MgO overlayers exhibited no Ni aggregation, like the SiO₂ overlayer shown in Fig. S4; however, the Ni coated with the TiO₂ overlayer exhibited severe aggregation of Ni nanoparticles, as shown in Fig. 7(l). Because the Ni nanoparticles retained their size, the support effect

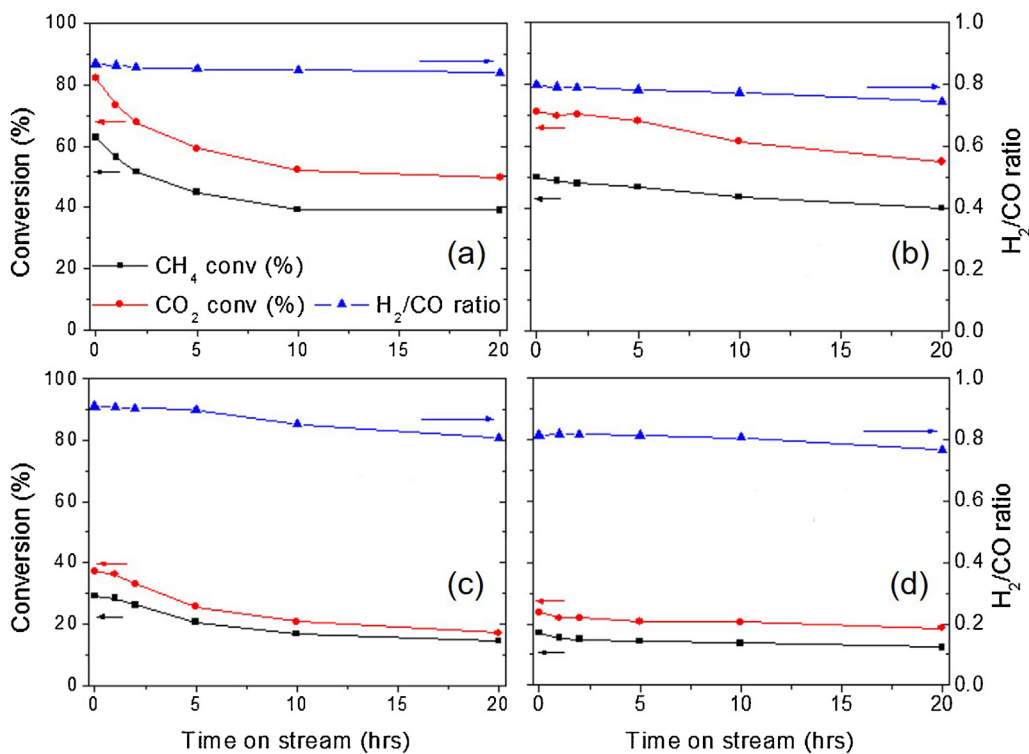


Fig. 9. CH₄ and CO₂ conversion and H₂/CO ratio results over catalysts coated with a) Al₂O₃, b) MgO, c) ZrO₂, and d) TiO₂ overlayers as a function of time on stream. (reaction conditions; 800 °C, 100 mg catalyst, the flow rates of CH₄, CO₂, and N₂ were 9, 9, and 2 mL/min, respectively.).

Table 2

The support effects of various metal oxide overlayer coatings on 5.2 nm Ni nanoparticles.

	Al ₂ O ₃	MgO	ZrO ₂	TiO ₂ ^a
Ni content (wt%)	0.23	0.26	0.32	0.21
Initial CO uptakes (μmol/g)	0.31	0.28	0.66	0.88
Initial CH ₄ Conversion (%)	62.8	50.0	29.1	17.0
Initial CO ₂ Conversion (%)	82.3	71.3	37.3	23.8
Initial TOF _{CH4} (s ⁻¹)	135.2	120.0	29.5	12.9
Initial TOF _{CO2} (s ⁻¹)	177.2	171.1	37.8	18.1

^a Severe Ni aggregation was observed prior to the reaction.

can be evaluated while excluding the Ni size effect for the Al₂O₃, ZrO₂, MgO, and SiO₂ overlayers.

The DRM reaction was performed over these catalysts, and the conversion results are shown in Fig. 9. The conversions decreased over time, indicating that deactivation occurred more easily than in the case of the SiO₂ overlayer. Therefore, only the initial turnover frequencies were compared for the different metal oxide overlayers. Table 2 shows the number of surface Ni sites and the turnover frequencies for the various metal oxide overlayers. The Al₂O₃ overlayer catalyst exhibited the highest turnover frequency. The turnover frequencies of each overlayer catalyst for methane conversion decreased in the order of Al₂O₃ > MgO > SiO₂ > ZrO₂ > TiO₂. In the case of TiO₂, the Ni nanoparticles severely aggregated; thus, the poor activity of this catalyst resulted from the large Ni domain size. When the initial turnover frequencies of SiO₂, Al₂O₃, MgO, and ZrO₂ were compared, Al₂O₃ and MgO exhibited much higher activities than SiO₂, as shown in Fig. 10. Basic supports are known to enable dissociative adsorption of CO₂ on the catalyst [24,26]. The enhanced activity of Al₂O₃ and MgO most likely results from greater CO₂ adsorption driven by their basic property. The amount of desorbed CO₂ estimated by CO₂-TPD was 33.7, 12.8, 7.6, 1.2, 2.1 μmol/g for Al₂O₃, MgO, ZrO₂, TiO₂, SiO₂, respectively. The Al₂O₃ overlay-

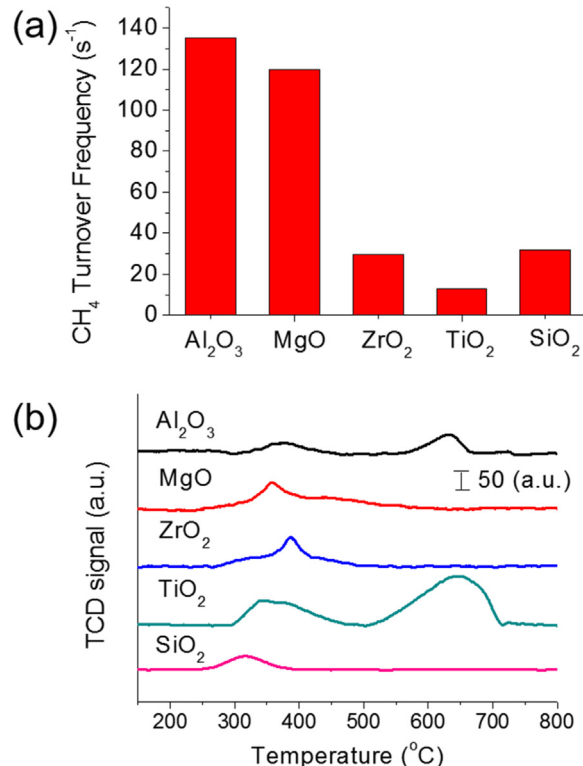


Fig. 10. (a) Dependence of CH₄ turnover frequency on the metal oxide overlayer on Ni/SiO₂, and (b) TPO results after running the DRM reaction at 800 °C for 20 h.

ers have more CO₂ adsorption comparing to other metal oxides. The CO₂-TPD results in Fig. S5 also show that CO₂ desorption peak for MgO appears at higher temperatures, indicating that CO₂ is more

strongly adsorbed. ZrO_2 exhibited activity similar to that of SiO_2 . ZrO_2 is known to have a high oxygen mobility, enabling the easy removal of the deposited carbon species [20,43]. However, ZrO_2 itself does not appear to enhance the catalytic activity.

TPO measurements were performed after running the DRM reaction for 20 h. Whereas MgO , ZrO_2 , and SiO_2 showed no peaks in the high temperature region ($\sim 600^\circ\text{C}$), the Al_2O_3 and TiO_2 overlayers did show a peak, indicating the presence of graphitic carbon on the catalysts. The sintered Ni on the TiO_2 catalyst produced the most carbon. The amphoteric Al_2O_3 overlayer with acidic sites also produced cokes with graphitic features [44]. TEM images of the Al_2O_3 and TiO_2 overlayers after the DRM reaction are shown in Fig. S6. Filamentous carbon can be clearly observed.

4. Conclusions

The Ni size effect and support effect were separately observed for the DRM reaction at 800°C . Four different sizes (2.6, 5.2, 9.0, and 17.3 nm) of Ni nanoparticles were prepared by wet chemistry and immobilized on silica spheres. A SiO_2 overlayer was subsequently coated onto the Ni nanoparticles. The Ni size changed little during 100 h of reaction at 800°C ; thus, the exact turnover frequency could be estimated for the various Ni particle sizes. The Ni nanoparticles with a diameter of 2.6 nm exhibited 4.1 times higher CH_4 turnover frequency than those with a diameter of 17.3 nm. Various metal oxide overlayers of Al_2O_3 , MgO , ZrO_2 , and TiO_2 were formed on Ni nanoparticles. A comparison of initial turnover frequencies revealed that Al_2O_3 and MgO , which have a basic surface property, exhibited higher turnover frequencies than the SiO_2 overlayer, whereas ZrO_2 exhibited a similar turnover frequency. The smaller Ni nanoparticles would definitely be more advantageous to ensuring high activity as long as the small size is preserved despite the high reaction temperature, and the interaction with basic supports can maximize the activity. This work provides a valuable design rule for developing catalysts for the DRM reaction that exhibit greater activity and stability.

Acknowledgements

This work was financially supported by the National Research Foundation of Korea (NRF-2015R1A2A2A01004467) funded by the Ministry of Education, Science and Technology and the Saudi Aramco-KAIST CO₂ Management Center. We also especially thank Prof. Ja Hun Kwak at UNIST for the valuable discussion about home-made TPD equipment.

Appendix A. Supplementary data

Supplementary data associated with this article can be found, in the online version, at <http://dx.doi.org/10.1016/j.apcatb.2016.10.069>.

References

- [1] E. Iglesia, *Appl. Catal. A-Gen.* 161 (1997) 59–78.
- [2] M.E. Dry, *Catal. Today* 71 (2002) 227–241.
- [3] G.W. Huber, S. Iborra, A. Corma, *Chem. Rev.* 106 (2006) 4044–4098.
- [4] A.Y. Khodakov, W. Chu, P. Fongarland, *Chem. Rev.* 107 (2007) 1692–1744.
- [5] M.C.J. Bradford, M.A. Vannice, *Catal. Rev.* 41 (1999) 1–42.
- [6] D. Pakhare, J. Spivey, *Chem. Soc. Rev.* 43 (2014) 7813–7837.
- [7] J.H. Kim, D.J. Suh, T.J. Park, K.L. Kim, *Appl. Catal. A-Gen.* 197 (2000) 191–200.
- [8] D. Chen, K.O. Christensen, E. Ochoa-Fernandez, Z.X. Yu, B. Toddal, N. Latorre, A. Monzon, A. Holmen, *J. Catal.* 229 (2005) 82–96.
- [9] S. Tang, L. Ji, J. Lin, H.C. Zeng, K.L. Tan, K. Li, *J. Catal.* 194 (2000) 424–430.
- [10] V.M. Gonzalez-Delacruz, F. Ternero, R. Pereniguez, A. Caballero, J.P. Holgado, *Appl. Catal. A-Gen.* 384 (2010) 1–9.
- [11] S.B. Wang, G.Q.M. Lu, *Appl. Catal. B-Environ.* 16 (1998) 269–277.
- [12] S.B. Zhang, J.K. Wang, H.T. Liu, X.L. Wang, *Catal. Commun.* 9 (2008) 995–1000.
- [13] K.Y. Koo, H.S. Roh, U.H. Jung, W.L. Yoon, *Catal. Lett.* 130 (2009) 217–221.
- [14] S. Corthals, J. Van Nederkassel, J. Geboers, H. De Winne, J. Van Noyen, B. Moens, B. Sels, P. Jacobs, *Catal. Today* 138 (2008) 28–32.
- [15] M.A. Naeem, A.S. Al-Fatesh, A.E. Abasaeed, A.H. Fakheha, *Fuel Process. Technol.* 122 (2014) 141–152.
- [16] V.M. Gonzalez-DelaCruz, J.P. Holgado, R. Pereniguez, A. Caballero, *J. Catal.* 257 (2008) 307–314.
- [17] Y.H. Wang, H.M. Liu, B.Q. Xu, *J. Mol. Catal. A-Chem.* 299 (2009) 44–52.
- [18] Q. Zhang, T. Wu, P. Zhang, R.J. Qi, R. Huang, X.F. Song, L. Gao, *RSC Adv.* 4 (2014) 51184–51193.
- [19] D. Baudouin, U. Rodemerck, F. Krumeich, A. de Mallmann, K.C. Szeto, H. Menard, L. Veyre, J.P. Candy, P.B. Webb, C. Thieuleux, C. Coperet, *J. Catal.* 297 (2013) 27–34.
- [20] A. Kambolis, H. Matralis, A. Trovarelli, C. Papadopoulou, *Appl. Catal. A-Gen.* 377 (2010) 16–26.
- [21] J.A.C. Dias, J.M. Assaf, *Catal. Today* 85 (2003) 59–68.
- [22] N. Wang, Z.X. Xu, J. Deng, K. Shen, X.P. Yu, W.Z. Qian, W. Chu, F. Wei, *ChemCatChem* 6 (2014) 1470–1480.
- [23] T. Horuchi, K. Sakuma, T. Fukui, Y. Kubo, T. Osaki, T. Mori, *Appl. Catal. A-Gen.* 144 (1996) 111–120.
- [24] J.S. Chang, S.E. Park, H.Z. Chon, *Appl. Catal. A-Gen.* 145 (1996) 111–124.
- [25] J. Juan-Juan, M.C. Roman-Martinez, M.J. Illan-Gomez, *Appl. Catal. A-Gen.* 301 (2006) 9–15.
- [26] A.A. Lemonidou, I.A. Vasalos, *Appl. Catal. A-Gen.* 228 (2002) 227–235.
- [27] H.S. Roh, K.W. Jun, *Catal. Surv. Asia* 12 (2008) 239–252.
- [28] N. Laosiripojana, S. Assabumrungrat, *Appl. Catal. A-Gen.* 290 (2005) 200–211.
- [29] S.M. Lima, J.M. Assaf, M.A. Pena, J.L.G. Fierro, *Appl. Catal. A-Gen.* 311 (2006) 94–104.
- [30] A. Peters, F. Nouroozzi, D. Richter, M. Lutecki, R. Glaser, *ChemCatChem* 3 (2011) 598–606.
- [31] H.S. Li, J.F. Wang, *Chem. Eng. Sci.* 59 (2004) 4861–4867.
- [32] B.Q. Xu, J.M. Wei, Y.T. Yu, Y. Li, J.L. Li, Q.M. Zhu, *J. Phys. Chem. B* 107 (2003) 5203–5207.
- [33] B.Q. Xu, J.M. Wei, Y.T. Yu, J.L. Li, Q.M. Zhu, *Top. Catal.* 22 (2003) 77–85.
- [34] Q.H. Zhang, L. Yan, B.Q. Xu, *Catal. Today* 98 (2004) 601–605.
- [35] L.B. Raberg, M.B. Jensen, U. Olsbye, C. Daniel, S. Haag, C. Mirodatos, A.O. Sjastad, *J. Catal.* 249 (2007) 250–260.
- [36] J.W. Han, C. Kim, J.S. Park, H. Lee, *ChemSusChem* 7 (2014) 451–456.
- [37] J. Park, E. Kang, S.U. Son, H.M. Park, M.K. Lee, J. Kim, K.W. Kim, H.J. Noh, J.H. Park, C.J. Bae, J.G. Park, T. Hyeon, *Adv. Mater.* 17 (2005) 429–434.
- [38] H. Winnischofer, T.C.R. Rocha, W.C. Nunes, L.M. Socolovsky, M. Knobel, D. Zanchet, *ACS Nano* 2 (2008) 1313–1319.
- [39] S. Okada, T. Kamegawa, K. Mori, H. Yamashita, *Catal. Today* 185 (2012) 109–112.
- [40] W. Stober, A. Fink, J. Colloid Interface Sci. 26 (1968) 62–69.
- [41] J.M. Wei, E. Iglesia, *J. Catal.* 224 (2004) 370–383.
- [42] R.V. Hardeveld, F. Hartog, *Surf. Sci.* 15 (1969) 189–230.
- [43] P. Djinovic, I.G.O. Crnivec, B. Erjavec, A. Pintar, *Appl. Catal. B-Environ.* 125 (2012) 259–270.
- [44] I.H. Son, S.J. Lee, A. Soon, H.S. Roh, H. Lee, *Appl. Catal. B-Environ.* 134 (2013) 103–109.